Analytical modeling of the pre– and post–yield behavior of bond in reinforced concrete

M. Fernández Ruiz[1] , A. Muttoni[2] and P. G. Gambarova[3]

Abstract: This paper presents the theoretical basis and the main results of an analytical model that describes the pre– and post–yield response of bond in reinforced concrete, as well as its influence on the behavior of structural members. The model is based on a number of reasonable assumptions that simplify the differential equation governing the phenomenon. In this way, a closed–form integration is feasible in certain cases, and relatively simple but accurate expressions can be worked out for the interface slip, the strain and the stress in the reinforcement and the bond stress at the bar–concrete interface. Applications are made to different structural members (pull–out specimens, tension ties and beams in bending), whose behavior is well documented in the literature. The agreement between the available test data turns out to be quite satisfactory. Consequently, the proposed model can be usefully adopted for studying the serviceability behavior, the ductility and the post–yield response of a variety of reinforced–concrete members.

CE Database subject headings: Bond stress; Slip; Reinforced concrete; Pull–out resistance; Tensile members; Anchorages.

[1]Post–doctoral fellow, Ecole Polytechnique Fédérale de Lausanne, IS–BETON, bât. GC, Station 18, CH-1015, Lausanne, Switzerland. E–mail: miguel.fernandezruiz@epfl.ch
[2]Professor, Ecole Polytechnique Fédérale de Lausanne, IS–BETON, bât. GC, Station 18, CH-1015, Lausanne, Switzerland. E–mail: aurelio.muttoni@epfl.ch
[3]Professor, Politecnico di Milano, DIS, Piazza Leonardo da Vinci 32, I-20133, Milan, Italy, E–mail: pietro.gambarova@polimi.it

Introduction

Most engineering problems concerning structural concrete have to do with bond, whose understanding and modeling is instrumental in treating such phenomena as tension–stiffening and cracking at the serviceability limit state, and structural ductility at the ultimate limit state (where the development of plastic strains in the reinforcement plays a major role).

The need for an analytical description of bond in the post–yield range of the reinforcement has led to the development of several theoretical models like that by Shima et al. (1987b, 1987c). More recently, a theory based on a rigid–plastic bond law has been proposed by Marti et al. (1998), and many models and test data have been presented and discussed in FIB Bulletin 10 (2000). Within this context, this paper summarizes the research activity of the authors.

As it is well known, bond mechanics in a uniaxial, axisymmetric problem can be modeled by means of a single second–order differential equation that has been written in different forms, in terms of bar slip or bar stress. However, the closed–form integration is possible only in a limited number of cases. In this paper a new approach to the problem is proposed on the basis of some reasonable assumptions that lead to the description of bond mechanics in long bonded members by means of a first–order differential equation. This equation can be easily integrated for any bond law, with reference to a wide range of practical applications.

Two bond–slip laws are considered in this study. The corresponding analytical expressions describing the strain and slip distributions for long pull–out specimens and tension ties include the pre– and post–yield behavior of the reinforcement. The resulting laws are simple enough to be used in practical cases, and satisfactorily fit the available test data.

Local bond stress law

This section describes the local response of bond considering two cases. In the first one, the slip along the axis of the bar is assumed to be constant (short bonded–length bars) while in the second case the slip is a function of the local coordinate (long bonded–length bars). Reference is made to an axisymmetric concrete cylinder reinforced with a single deformed bar, that is assumed to be well confined. Thus, cover splitting is neglected and consequently the theory developed can be applied to specimens where the ratio between the concrete cover and the bar diameter is larger than 3 (Schenkel 1998). Also, size effect is neglected (Bamonte et al. 2004).

When the bonded length of an embedded bar is relatively small ($L<5\phi_s$) and a force F is applied at one of its ends, the relative steel–concrete slip can be considered constant in the longitudinal direction. The bar behaves like a rigid body with a similar response regardless of the type of bond test performed (pull–out or push–in test). The response, see figure 1 (a), is characterized by an ascending branch up to a certain relative slip where the force reaches its maximum, followed by a softening branch.

The similarity of the behavior in pull–out and push–in tests can be explained by the relatively low stresses and strains in the bar. Consequently, the response of the system is mainly controlled by the strength of the surrounding concrete, as well as by the geometry of the ribs. A one–to–one relationship can be formulated between the average bond stress and the relative slip:

$$\tau_s(\delta) = \frac{F(\delta)}{\pi \cdot \phi_s \cdot L} \tag{1}$$

where δ is the relative bar slip.

However, when the bonded length is relatively large (typically $L>10\phi_s$), the steel strains cannot be neglected and the slip between the bar and the concrete block cannot be considered

constant. This is a very typical situation in reinforced concrete, since many codes specify minimum values for L/ϕ_s larger than 10.

In this case, the local response of bond is affected at each point by the longitudinal strain state of the bar (ε_s). For instance, see figure 1 (b), for large tensile strains in the bar, bond efficiency is decreased by the lateral contraction of the bar, while for large negative strains it is increased by the lateral expansion of the bar, which improves the wedging effect of the ribs (known as Hoyer's effect). In order to include this phenomenon in the local bond stress–slip law, it is proposed to introduce a bond coefficient (K_b) which locally corrects the previously–defined bond stress for short specimens:

$$\tau(\delta, \varepsilon_s) = \tau_s(\delta) \cdot K_b(\varepsilon_s) \tag{2}$$

However, the bond stress in long anchored bars cannot be fully developed in certain cases, as –for instance– when the ribs cause a local punching shear failure, because of the development of conical microcracks (see figure 1 (c)), that propagate up to the free surface of the concrete. This case is typical of some structural members like for instance tension ties close to their ends or close to intermediate cracks (this effect depends on the load level of the bar and on the size of the member). For other test set–ups (for instance pull–out tests) this mechanism of local punching cannot be developed because of the compressive stresses introduced by the bearing plate (see figure 1 (a)).

To introduce this effect in the local bond model, it is proposed to adopt an "effectiveness" parameter $\lambda(x/\phi_s)$ that reduces the local bond stress in the following way:

$$\tau(\delta, \varepsilon_s, x) = \tau_s(\delta) \cdot K_b(\varepsilon_s) \cdot \lambda(x/\phi_s) \tag{3}$$

where x is the distance from the loaded end (see figure 1c) and $\lambda(x/\phi_s)$ is ≤ 1. If $\lambda(x/\phi_s)$ is smaller than 1, then the local punching of the ribs plays a major role, whereas this effect can be neglected when λ is equal to 1.

Affinity of the slip distribution in long anchored bars

Bond differential equation

With reference to a unidimensional system consisting of a bar and a concrete prism or cylinder, the differential equation governing bond response can be obtained from the equilibrium of an infinitesimal element as shown in figure 2. If the sum of the forces acting on the bar is performed, the following relationship is obtained:

$$\frac{\pi}{4}\cdot\phi_s^2\cdot d\sigma_s = -\tau\cdot\pi\cdot\phi_s\cdot dx \rightarrow \frac{d\sigma_s}{dx} = -\frac{4\cdot\tau}{\phi_s} \tag{4}$$

For any given constitutive law of the steel ($\sigma_s=\sigma_s(\varepsilon_s)$), equation (4) can be rewritten as:

$$\frac{d(\sigma_s(\varepsilon_s))}{dx} = -\frac{4\cdot\tau}{\phi_s} \tag{5}$$

In order to easily integrate equation (5) in fully anchored bars, an assumption can be made on the shape of the $\delta(x)$ curves.

Affinity of the $\delta(x)$ curves

The qualitative slip distribution along the axis of an anchored bar is shown in figure 3, with reference to two load steps. The slip distribution in the second load step (maximum slip δ_j) is assumed to be the same as in the first load step for ξ in (0; x_i). This implies that there is a unique $\delta(\xi)$ law for the whole bar, regardless of the load level. As a consequence, δ can be seen solely as a function of the length of the zone where bond is active, and so $\delta = \delta(x)$. The relative slip can be calculated in a general way at x as follows:

$$\delta = \int_0^x (\varepsilon_s(\xi) - \varepsilon_c(\xi))d\xi = \delta(x) \tag{6}$$

By neglecting the concrete strains (much smaller than the steel strains) and by deriving both sides, the following equation is obtained:

$$\frac{d\left(\int_0^x \varepsilon_s(\xi)d\xi\right)}{dx} = \frac{d(\delta(x))}{dx} \rightarrow \varepsilon_s(x) = \delta'(x) \tag{7}$$

Since $\delta(x)$ and $\varepsilon_s(x)$ are both functions of x, then it can be stated that $\delta = \delta(\varepsilon_s)$. Based on this statement, the local $\tau_s(\delta)$ law can be formulated in terms of ε_s:

$$\tau_s(\delta) = \tau_s(\varepsilon_s) \tag{8}$$

By introducing this relationship into equation (3), equation (5) can be formulated in the following way:

$$\frac{d(\sigma_s(\varepsilon_s))}{\tau_s(\varepsilon_s)\cdot K_b(\varepsilon_s)\cdot\lambda(x/\phi_s)} = -\frac{4}{\phi_s}dx \tag{9}$$

leading to the following first–order differential equation:

$$\frac{\sigma_s'(\varepsilon_s)}{\tau_s(\varepsilon_s)\cdot K_b(\varepsilon_s)}d\varepsilon_s = -\frac{4\cdot\lambda(x/\phi_s)}{\phi_s}dx \tag{10}$$

Applicability of the affinity hypothesis

The previous assumption on affinity among the $\delta(x)$ curves is in principle satisfied only by fully–anchored bars. Deviations from this assumption occur in other cases as shown in figure 4c for a pull–out specimen (left side of the figure) and a tension tie (right side of the figure). However, the deviations for these members are usually limited as it will be shown later.

If the affinity hypothesis is satisfied, the local $\tau_s(\delta)$ law (which neglects the strains in the bar and the effects of local punching) can be obtained for any given $\tau_s(\varepsilon_s)$ law and vice versa, by adopting $K_b = \lambda = 1$. To do this, equation (10) has to be integrated obtaining $\varepsilon_s(x)$; the relative slip $\delta(x)$ is worked out by integrating $\varepsilon_s(x)$:

$$\delta = \int_0^x \varepsilon_s(\xi)d\xi \tag{11}$$

Finally, by eliminating x from the previous expressions, the $\delta(\varepsilon_s)$ law is obtained and the bond stress can be expressed as a function of the slip: $\tau_s(\delta)$. For instance, it can be easily demonstrated that a function of the type $\tau_s = k_1 \varepsilon_s^{1/\alpha}$ is generated by $\tau_s = k_2 \delta^{1/(2\alpha - 1)}$. Within this approach, various analytical laws can be proposed. Because of their simplicity and good agreement with experimental results, two laws are presented in the following (corresponding to $\alpha = 2$, square–root model, and $\alpha \to \infty$, rigid–plastic model), as shown in figure 5.

Square–Root Model

Starting from a third–root relationship between τ_s and δ ($\tau_s \propto \delta^{1/3}$ which can be considered rather realistic as discussed by Laurencet, 1999) and using the hypothesis of affinity among the $\delta(x)$ curves, the corresponding $\tau_s(\varepsilon_s)$ law is obtained:

$$\tau_s(\varepsilon_s) = \tau_{ref} \sqrt{\varepsilon_s} \tag{12}$$

A good agreement of the analytical model with experimental results is obtained using $\tau_{ref} = \tau_{b,\max} \Big/ \sqrt{\varepsilon_y}$ (where $\tau_{b,max} = f_c^{2/3}$). To introduce the influence of the longitudinal strains of the bar, the following bond coefficient is adopted:

$$\begin{cases} 0 < \varepsilon_s \le \varepsilon_{bu} & K_b(\varepsilon_s) = \dfrac{\varepsilon_{bu} - \varepsilon_s}{\varepsilon_{bu} - \varepsilon_y} \sqrt{\dfrac{\varepsilon_y}{\varepsilon_s}} \le 1 \\ \varepsilon_s > \varepsilon_{bu} & K_b(\varepsilon_s) = 0 \end{cases} \tag{13}$$

where the parameter ε_{bu} is mainly influenced by the rib height and by the hardening modulus of the bar. A good correlation with experimental results has been found by adopting $\varepsilon_{bu} = 4a/\phi_s$ (the usual range is from 0.07 to 0.12), where a is the rib height. By adopting the aforementioned formulation for the bond coefficient K_b and by introducing the effect of the local punching of the ribs, the relationship between τ_s, ε_s, and x can be finalized as follows:

$$\begin{cases} 0 < \varepsilon_s \le \varepsilon_y & \tau = \tau_{b,\max} \sqrt{\dfrac{\varepsilon_s}{\varepsilon_y}} \cdot \lambda(x/\phi_s) \\ \varepsilon_y < \varepsilon_s (< \varepsilon_{bu}) & \tau = \tau_{b,\max} \dfrac{\varepsilon_{bu} - \varepsilon_s}{\varepsilon_{bu} - \varepsilon_y} \cdot \lambda(x/\phi_s) \end{cases} \tag{14}$$

Rigid–Plastic Model

A simplified model, based on a rigid–plastic bond–slip law is also studied in this paper. The corresponding bond stress–bar strain law is rigid–plastic as well ($\tau_s = \tau_0$). The following expression is adopted for the bond coefficient:

$$K_b = \exp\left[A \cdot (\varepsilon_y - \varepsilon_s)\right] \tag{15}$$

The parameter A depends on rib geometry and on steel–hardening properties; however, a reasonable agreement with the experimental data is found for $A = 10$. With this value, by introducing the reduction due to local punching, the bond strain law can be expressed as follows:

$$\begin{cases} 0 < \varepsilon_s \le \varepsilon_y & \tau = \tau_0 \cdot \lambda(x/\phi_s) \\ \varepsilon_s > \varepsilon_y & \tau = \tau_0 \cdot \exp\left[A \cdot (\varepsilon_y - \varepsilon_s)\right] \cdot \lambda(x/\phi_s) \end{cases} \tag{16}$$

For τ_0 the value $0.6\, f_c^{2/3}$ has been adopted, as proposed by Marti et al. (1998).

Pull–out tests on long anchored bars

In this section, the proposed analytical model is applied to long anchored bars, whose pull–out response is studied on the basis of the affinity hypothesis.

In order to model a long bar subjected to pull–out, the previous bond laws are used, and a bilinear formulation with constant strain hardening for the reinforcing bar is adopted, as sketched in figure 6. The local punching of concrete is not considered in this test set–up ($\lambda = 1$), as previously discussed.

Analytical results

The proposed approach is used to study two different cases, the first with a fully–elastic bar and the second with a partially–yielded bar.

Bar in the elastic domain ($\varepsilon_s < \varepsilon_y$)

The strain and the slip can be expressed as a function of the distance x from the loaded end (as sketched qualitatively in figure 7). The Square–Root model and the Rigid–Plastic model lead to the following expressions for ε_s and δ:

$$\text{Square - Root Model} \begin{cases} \varepsilon_s = \left(\sqrt{\varepsilon_0} - \dfrac{2 \cdot \tau_{b,\max} \cdot x}{E_s \cdot \phi_s \cdot \sqrt{\varepsilon_y}} \right)^2 \\ \delta = \dfrac{E_s \cdot \phi_s \cdot \sqrt{\varepsilon_y}}{6 \cdot \tau_{b,\max}} \cdot \left(\sqrt{\varepsilon_0} - \dfrac{2 \cdot \tau_{b,\max} \cdot x}{E_s \cdot \phi_s \cdot \sqrt{\varepsilon_y}} \right)^3 \end{cases} \tag{17}$$

$$\text{Rigid - Plastic Model} \begin{cases} \varepsilon_s = \varepsilon_0 - \dfrac{4 \cdot \tau_0 \cdot x}{E_s \cdot \phi_s} \\ \delta = \varepsilon_0 \left(\dfrac{E_s \cdot \phi_s \cdot \varepsilon_0}{4 \cdot \tau_0} - x \right) - \dfrac{2 \cdot \tau_0}{E_s \cdot \phi_s} \cdot \left(\left(\dfrac{E_s \cdot \phi_s \cdot \varepsilon_0}{4 \cdot \tau_0} \right)^2 - x^2 \right) \end{cases} \tag{18}$$

Bar in the elasto–plastic domain

For any load larger than that causing the yielding at the loaded end, the bar is partly in the plastic domain (l_p; $\varepsilon_s > \varepsilon_y$) and partly in the elastic domain ($l - l_p$; $\varepsilon_s \leq \varepsilon_y$), see the qualitative sketch of figure 8.

The elastic strains ($\varepsilon_{s,e}$) are evaluated by using the equations (17) and (18) respectively, where $\varepsilon_0 = \varepsilon_y$. As for the plastic zone, the differential equation is integrated again to obtain the plastic strains in the bar ($\varepsilon_{p,e}$).

Square–Root Model:

$$\begin{cases} \varepsilon_s = \begin{cases} \left(\sqrt{\varepsilon_y} - \dfrac{2\cdot\tau_{b,\max}\cdot(x-l_p)}{E_s\cdot\phi_s\cdot\sqrt{\varepsilon_y}}\right)^2 & x > l_p \\ \varepsilon_{bu} - (\varepsilon_{bu}-\varepsilon_y)\cdot\exp\left[\dfrac{4\cdot\tau_{b,\max}\cdot(x-l_p)}{E_h\cdot\phi_s\cdot(\varepsilon_{bu}-\varepsilon_y)}\right] & x \le l_p \end{cases} \\ \delta = \begin{cases} \dfrac{E_s\cdot\phi_s\cdot\sqrt{\varepsilon_y}}{6\cdot\tau_{b,\max}}\left(\sqrt{\varepsilon_y} - \dfrac{2\cdot\tau_{b,\max}\cdot(x-l_p)}{E_s\cdot\phi_s\cdot\sqrt{\varepsilon_y}}\right)^3 & x > l_p \\ \dfrac{f_y\cdot\phi_s\cdot\varepsilon_y}{6\cdot\tau_{b,\max}} + \varepsilon_{bu}\cdot(l_p-x) - \dfrac{\phi_s\cdot E_h\cdot(\varepsilon_{bu}-\varepsilon_y)^2}{4\cdot\tau_{b,\max}}\left(1-\exp\left[\dfrac{4\cdot\tau_{b,\max}\cdot(x-l_p)}{E_h\cdot\phi_s\cdot(\varepsilon_{bu}-\varepsilon_y)}\right]\right) & x \le l_p \end{cases} \end{cases} \quad (19)$$

Rigid–Plastic Model:

$$\begin{cases} \varepsilon_s = \begin{cases} \varepsilon_y - \dfrac{4\cdot\tau_0\cdot(x-l_p)}{E_s\cdot\phi_s} & x > l_p \\ \varepsilon_y + \dfrac{1}{A}\cdot\log\left[1+\dfrac{4\cdot\tau_0\cdot A\cdot(l_p-x)}{E_h\cdot\phi_s}\right] & x \le l_p \end{cases} \\ \delta = \begin{cases} \varepsilon_y\cdot\left(\dfrac{f_y\cdot\phi_s}{4\cdot\tau_0}-(x-l_p)\right) - \dfrac{2\cdot\tau_0}{E_s\cdot\phi_s}\cdot\left(\left(\dfrac{f_y\cdot\phi_s}{4\cdot\tau_0}\right)^2-(x-l_p)^2\right) & x > l_p \\ \dfrac{f_y\cdot\phi_s\cdot\varepsilon_y}{8\cdot\tau_0} + \varepsilon_y\cdot(l_p-x) + \dfrac{1}{A}\cdot\left((x-l_p)+\log\left[1+\dfrac{4\cdot\tau_0\cdot A\cdot(l_p-x)}{E_h\cdot\phi_s}\right]\cdot\left(\dfrac{\phi_s\cdot E_h}{4\cdot\tau_0\cdot A}+(l_p-x)\right)\right) & x \le l_p \end{cases} \end{cases} \quad (20)$$

Experimental results

In this section, the analytical results are compared with tests performed on long anchored bars by various researchers.

Elastic behavior of the bar

To study the response of a long anchored bar in the elastic domain, Shima et al. (1987a) performed a series of pull–out tests on steel and aluminum bars embedded in ordinary concrete (f_c = 34 MPa). All bars had a diameter of 17.7 mm and the bonded length was equal to 40ϕ_s. The material properties were E_s = 190 GPa and $f_{y,s}$ = 480 MPa for the steel, and E_a = 70 GPa and $f_{y,a}$ = 450 MPa for the aluminum.

The results were presented in terms of $\tau(\delta)$ curves. With the proposed approach, this relationship can be obtained by eliminating x from equations (17) and (18). The Square–Root Model leads to the following expression for τ:

$$\tau = \frac{\tau_{b,\max}}{\sqrt{\varepsilon_y}} \left[\frac{6 \cdot \tau_{b,\max} \cdot \delta}{E_s \cdot \phi_s \cdot \sqrt{\varepsilon_y}} \right]^{1/3} \tag{21}$$

whereas in the case of the Rigid–Plastic Model τ is constant: $\tau = \tau_0$.

In figure 9, the results of the analytical model are compared with those by Shima et al. The Square–Root Model correctly reproduces the evolution of the bond stress for the different values of the elastic modulus of the bar. The Rigid–Plastic Model provides a reasonable estimate of the mean value of the bond stress, but does not describe the actual bond–stress distribution.

Elasto–plastic behavior of the bar

Shima et al. (1987b) performed several tests on long anchored bars, to study the effects of the post–yield behavior of the reinforcing bars. Figure 10 shows Shima's results, as well as those obtained by means of the analytical model. Reference is made to specimen SD70 (where for the proposed model it has been considered: ϕ_s = 19.5 mm; $\tau_{b,\max}$ = 8 MPa and ε_{bu} = 0.07). On the whole, the agreement is satisfactory, but certain differences are found in the strains at the loaded end of the bar (where the analytical models predict shorter plasticized zones).

Bigaj (1995) also performed several tests on long anchored bars to study the post–yield response of a reinforcing bar. The plots of the steel strains along the axis of the bar (figure 11) show a good agreement among the tests and the analytical models (ϕ_s = 16 mm; $\tau_{b,\max}$ = 10 MPa and ε_{bu} = 0.12).

Tension tie

As previously discussed with reference to the coefficient λ, the formation of roughly conical cracks radiating from the ribs closest to the end sections leads to a local loss of bond stiffness and strength. The same phenomenon occurs in reinforced–concrete beams, since conical cracks radiate from the ribs of the tension bars, close to the flexural cracks.

Analytical model

The phenomenon of local punching is now taken into account by introducing the parameter $\lambda(x/\phi_s)$. Since the influence of this coefficient on the global response of a tie is rather small and any more or less complex formulation can hardly take into account the load level and the size of the specimen, a simplified formulation is adopted here:

$$\lambda(x/\phi_s) = 1 - \exp\left[-\frac{x}{\phi_s}\right] \tag{22}$$

Furthermore, as long as the bar remains in the elastic domain, the influence of this phenomenon can be neglected, since cracking at the end sections is very limited. On the contrary, bond loss at the ends of a tie cannot be neglected after the yielding of the bar. In the plastic case, the differential equation can be integrated as seen earlier, and the following expressions are obtained:

Square–Root Model:

$$\varepsilon_s = \begin{cases} \left(\sqrt{\varepsilon_y} - \dfrac{2\cdot\tau_{b,\max}\cdot(x-l_p)}{E_s\cdot\phi_s\cdot\sqrt{\varepsilon_y}}\right)^2 & x > l_p \\ \varepsilon_{bu} - (\varepsilon_{bu}-\varepsilon_y)\cdot\exp\left[\dfrac{4\cdot\tau_{b,\max}}{E_h\cdot\phi_s\cdot(\varepsilon_{bu}-\varepsilon_y)}\cdot\left((x-l_p)-\phi_s\cdot\left(\exp\left[-\dfrac{l_p}{\phi_s}\right]-\exp\left[-\dfrac{x}{\phi_s}\right]\right)\right)\right] & x \le l_p \end{cases} \tag{23}$$

Rigid–Plastic Model:

$$\varepsilon_s = \begin{cases} \varepsilon_y - \dfrac{4 \cdot \tau_0 \cdot (x - l_p)}{E_s \cdot \phi_s} & x > l_p \\ \varepsilon_y + \dfrac{1}{A} \cdot \log\left[1 + \dfrac{4 \cdot \tau_0 \cdot A}{E_h \cdot \phi_s}\left((l_p - x) + \phi_s \cdot \left(\exp\left[-\dfrac{l_p}{\phi_s}\right] - \exp\left[-\dfrac{x}{\phi_s}\right]\right)\right)\right] & x \le l_p \end{cases} \quad (24)$$

Experimental results

A few experimental results concerning tension ties and tension chords in beams loaded in bending are considered here to make comparisons with the proposed analytical model. Both the elastic and the plastic cases are considered.

Elastic behavior of the bar

The results obtained by means of the proposed model in the elastic domain are compared with those obtained on 25–mm cold–worked ribbed bars (E_s = 200 GPa, concrete cube strength f_{cw} = 50 MPa) by Kankam (1997). The distribution of the strains along one half of the tie is shown in figure 12. The Square–Root Model fits quite well the test results, while the Rigid–Plastic Model tends to underestimate the steel strain at small slip values. In figure 12 (c) the bar maximum stress is plotted versus the mean strain, and the response of a naked bar is also shown to visualize tension–stiffening effects, that are is well reproduced by the square–root model and satisfactorily approximated by the rigid–plastic model.

Elasto–plastic behavior of the bar

Kenel and Marti (2001) carried out a series of tests on five reinforced– and prestressed–concrete beams where the strains were measured by means of Bragg grating sensors. These beams were loaded in four–point bending and presented a pure–bending zone between the supports. The post–yield behavior of the reinforcement was studied (Kenel 2002), in order to make comparisons with several theoretical models (Shima et al. 1987c; CEB 1993; Alvarez 1998).

Figure 13 refers to three load steps of specimen B4 (ϕ_s = 10 mm; $\tau_{b,\max}$ = 8 MPa and ε_{bu} = 0.10). The bond stress decreases at the ends as indicated by the decreasing slope of the steel–strain diagrams. In general, the Square–Root Model yields better results than the Rigid–Plastic Model.

Shima et al. (1987c) carried out an experimental campaign on reinforced ties to study their post–yield response. In figure 14, the results obtained with the proposed approach for P/P_{yield} = 1.08 are shown to fit quite well the test results (specimen No. 4; ϕ_s = 19.5 mm; $\tau_{b,\max}$ = 7 MPa and ε_{bu} = 0.07).

Conclusions

This paper is aimed at the analytical modeling of bond in long anchored bars and tension ties, with reference to the pre– and post–yield behaviors of the steel. A new approach is proposed, on the assumption that:

(a) bond is locally influenced by the lateral expansion/contraction of the bar.

(b) bond strength and stiffness are locally controlled by the development of conical cracks close to the loaded end of an anchored bar, to both ends in a tension tie and to the flexural cracks in the tension chord of a reinforced–concrete beam subjected to bending.

(c) affinity controls the distribution of the bar–concrete slip at different load levels for fully–anchored members.

These assumptions make it possible to downsize the problem, since the integration of the second–order differential equation of bond (where the unknown is the steel stress) is replaced by the integration of a first–order differential equation (where the unknown is the steel strain). This equation can be integrated in a closed form in several cases, and the response of the anchored bar is described by simple analytical expressions.

Because of the affinity between the bond stress and the bar slip, and between the bond stress and the steel strain, the equation can be integrated for any given bond–stress/slip law. In this paper, starting from two bond–stress/bar slip laws, two bond–stress/steel strain relations are obtained (named Square–Root Model and Rigid–Plastic Model).

Finally, the simplicity of the proposed approach allows to perform a detailed study of the pre– and post–yield behavior of bond in anchored bars and tension ties, with the advantage over finite element modeling that the role of the various mechanical and geometrical parameters can be clearly assessed. The proposed approach can thus be adopted in practical cases, at the service limit state (where tension–stiffening effects are properly reproduced) as well as at the ultimate limit state, where the ductility and post–yield response of a reinforced member is also rather well reproduced.

Notation

The following symbols are used in this paper:

a = rib height

E_a = elastic modulus of an aluminum rebar

E_s = elastic modulus of any rebar, and specifically of a steel rebar

E_h = hardening modulus of the steel

F = force

f_c = concrete cylindrical compressive strength

f_y = steel strength at yielding

K_b = bond coefficient

L = bonded length

l_p = plasticized length of a bonded bar

δ = relative bar–concrete slip

δ_e = relative slip prior to bar yielding

δ_p = relative slip past bar yielding

δ_y = relative slip at the onset of bar yielding

ε_s = strain in a rebar

$\varepsilon_{s,e}$ = elastic strain in a rebar

$\varepsilon_{s,p}$ = plastic strain in a rebar

ε_y = steel strain at yielding

ε_{bu} = bond ultimate strain

ϕ_s = bar diameter

λ = local punching coefficient

σ_s = stress in a steel bar

τ = bond stress

τ_0 = reference bond stress in the rigid–plastic model

τ_s = bond stress in short anchored bars

$\tau_{b,\max}$ = maximum bond stress

References

Alvarez, M. (1998). "Influence of bond behavior on the deformation capacity of reinforced concrete" (in German, "Einfluss des Verbundverhaltens auf das Verformungsvermögen von Stahlbeton"), *ETHZ, Swiss Federal Institute of Technology Zürich,* Report No. 236, Birkhäuser, Basel-Boston-Berlin, Switzerland, 182 p.

Bamonte P., Coronelli, D. and Gambarova, P. G. (2004). "Local bond–stress/slip law and size effect in high–bond bars", *Proc. 5th Int. Conf. on Fracture Mechanics of Concrete and Concrete Structures – FRAMCOS'5*, Vail (Colorado, USA), Vol. 2, pp. 869–876.

Bigaj, A. J. (1995). "Bond behaviour of deformed bars in NSC and HSC. Experimental study", *Faculty of Civil Engineering, Delft University of Technology*, Report 25.5–95–II, Delft, The Netherlands, 132 p.

CEB–FIP (1993) "Model code 1990 for concrete structures", *Comité Euro–International du Béton (Lausanne, Switzerland)*, Thomas Telford, London, 437 p.

FIB (2000) "Bond of reinforcement in concrete", *Fédération Internationale du Béton (Lausanne, Switzerland),* Bulletin No. 10, Sprint-Druck, Stuttgart, 427 p.

Kankam, C. K. (1997). "Relationship of bond stress, steel stress, and slip in reinforced concrete", *Journal of Structural Engineering*, ASCE, Vol. 123, No 1, pp. 79–85.

Kenel, A., and Marti, P. (2001). "Optic–fibre strain measurements in embedded reinforcing bars" (in German, "Faseroptische Dehnungsmessungen an einbetonierten Bewehrungsstäben"), *ETHZ, Swiss Federal Institute of Technology Zürich,* Report No. 271, Birkhäuser, Basel-Boston-Berlin, Switzerland, 93 p.

Kenel, A. (2002). "Flexural behaviour and minimal reinforcement in reinforced concrete structural elements" (in German, "Biegetragverhalten und Mindestbewehrung von

Stahlbetonbauteilen"), *ETHZ, Swiss Federal Institute of Technology Zürich,* phD. Thesis 14874, Zürich, Switzerland, 115 p.

Laurencet, P. (1999). "Prestressing and minimal reinforcement for the control of the residual crack width" (in French, "Précontrainte et armature pour contrôler l'ouverture résiduelle des fissures"), *EPFL, Swiss Federal Institute of Technology Lausanne,* phD. Thesis 2028, Lausanne, Switzerland, 258 p.

Marti, P., Alvarez. M., Kaufmann, W. and Sigrist, V. (1998). "Tension chord model for structural concrete", *Structural Engineering International*, *IABSE*, Vol 8, No 4, Switzerland, pp. 287–298.

Schenkel, M. (1998) "On bond behavior of reinforcing bars with limited cover" (in German, "Zum Verbundverhalten von Bewehrung bei kleiner Betondeckung"), *ETHZ, Swiss Federal Institute of Technology Zürich,* Report No. 237, Birkhäuser, Basel-Boston-Berlin, Switzerland, 162 p.

Shima, H., Chou, L–L. and Okamura, H. (1987a). "Bond–slip–strain relationship of deformed bars embedded in massive concrete", *Concrete Library of JSCE*, (Translation from Proceedings of JSCE, No 378/V-6), No 10, Japan, pp. 79–94.

Shima, H., Chou, L–L. and Okamura, H. (1987b) "Bond characteristics in post–yield range of deformed bars", *Concrete Library of JSCE*, (Translation from Proceedings of JSCE, No 378/V-6), No 10, Japan, pp. 113–124.

Shima, H., Chou, L–L. and Okamura, H. (1987c). "Micro and macro models for bond in reinforced concrete", *Journal of the Faculty of Engineering*, University of Tokyo, Vol. XXXIX, No 2, Japan, pp. 133–194.

Sigrist, V. (1995). “On the deformation capacity of reinforced concrete girders” (in German, “Zum Verformungvermögen von Stahlbetonträgern”), *ETHZ, Swiss Federal Institute of Technology Zürich,* Report No. 210, Birkhäuser, Basel-Boston-Berlin, Switzerland, 159 p.

Figure captions

Figure 1: Local bond law: (a) response of a short anchored bar; (b) influence of the longitudinal strain of the bar (ε_s) and coefficient K_b; and (c) local punching of outer ribs and coefficient λ for a long anchored bar.

Figure 2: Equilibrium of a reinforcing bar: (a) actual forces ($F_{s,A} > F_{s,B}$); and (b) simplified state of stress.

Figure 3: Relative slip along the axis of a bar at different load levels.

Figure 4: Applicability of the affinity hypothesis: (a) pull–out specimen and tension tie; (b) slip evolution according to the affinity hypothesis; and (c) actual behavior.

Figure 5: Bond laws and bond coefficients for f_c = 30 MPa, E_s = 210 GPa and f_y = 500 MPa: (a) $\tau(\delta)$ laws; (b) bond coefficient; and (c) $\tau(\varepsilon_s)$ laws.

Figure 6: Simplified stress–strain law for a steel bar.

Figure 7: Strain and slip distributions along the axis of a long anchored bar in the elastic domain.

Figure 8: Plastic length (l_p), and strain and slip distributions along the axis of a long anchored bar in the elasto–plastic domain.

Figure 9: Tests by Shima et al. (1987a): (a) test set–up; (b) steel bar (E_s = 190 GPa); and (c) aluminum bar (E_a = 70 GPa).

Figure 10: Fitting of the test results by Shima et al. (1987b, test SD70): (a) test set–up; (b) stress, strain and slip distributions along the axis of the bar at the last load step (P/P_{yield} = 1.05); and (c) plots of the bond stress, slip and axial strain.

Figure 11: Fitting of the test results by Bigaj (1995, test 16.16.1): (a) test set–up; (b) plots at different load levels (ε_y = 0.26 % in the authors' model); and (c) detail of the plasticized zone at increasing load levels.

Figure 12: Fitting of the test results by Kankam (1997): (a) test set–up; (b) plots at different load levels; and (c) tension–stiffening effect in the tie.

Figure 13: Fitting of the test results by Kenel and Marti (2001, test B4): (a) test set–up; (b) plots of the steel strain for various load levels; and (c) τ - ε_s - δ diagrams.

Figure 14: Plots of the strains in the rebar of specimen No. 4 by Shima et al. (1987c) at P/P_{yield} = 1.08: (a) test set–up; (b) square–root model; and (c) rigid–plastic model.

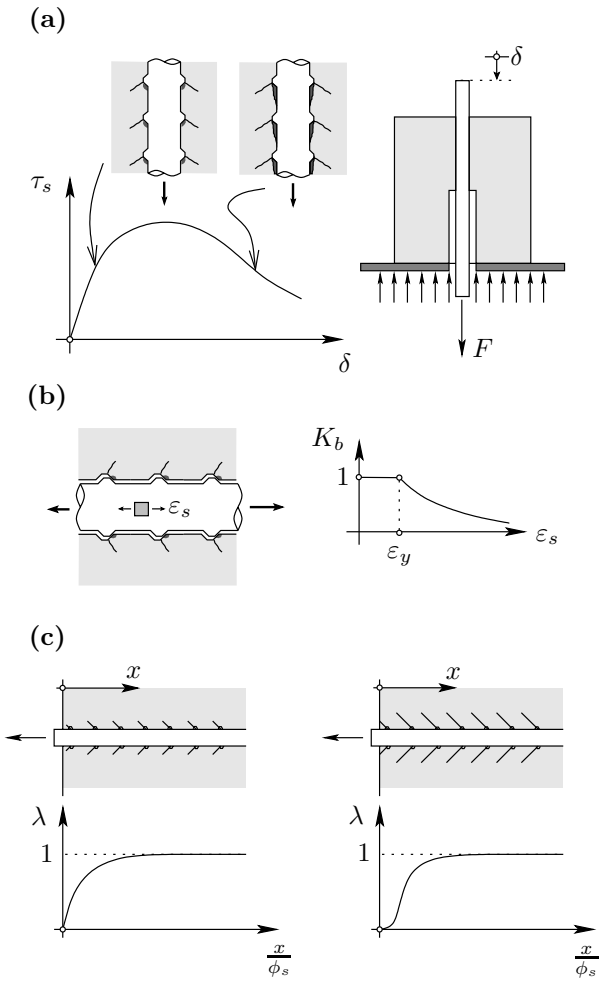

Figure 1

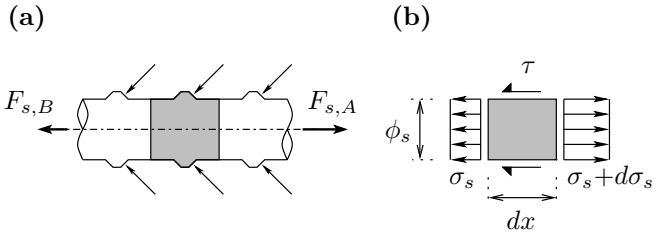

Figure 2

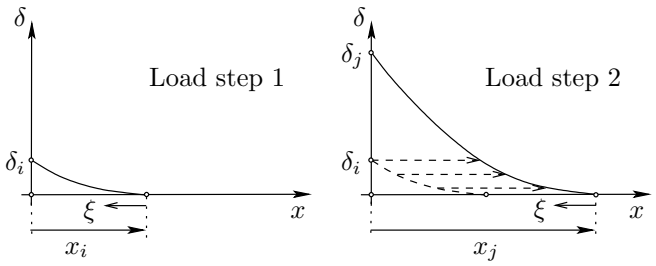

Figure 3

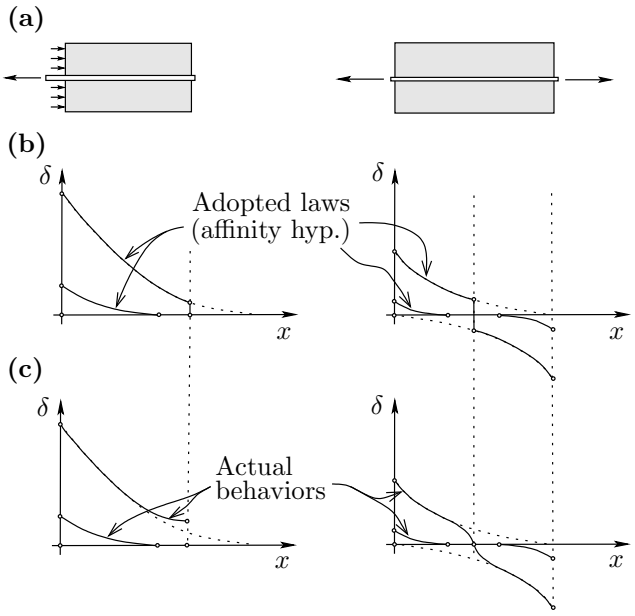

Figure 4

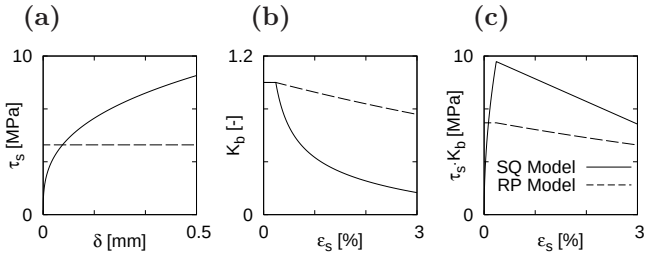

Figure 5

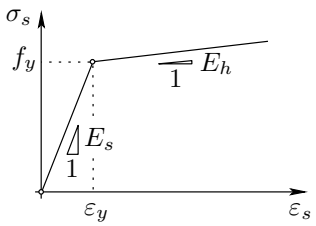

Figure 6

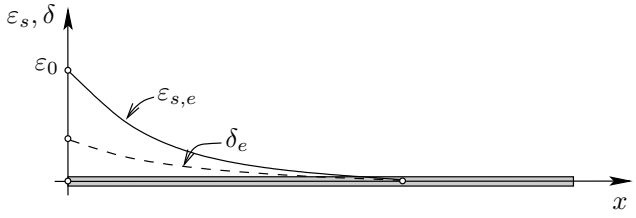

Figure 7

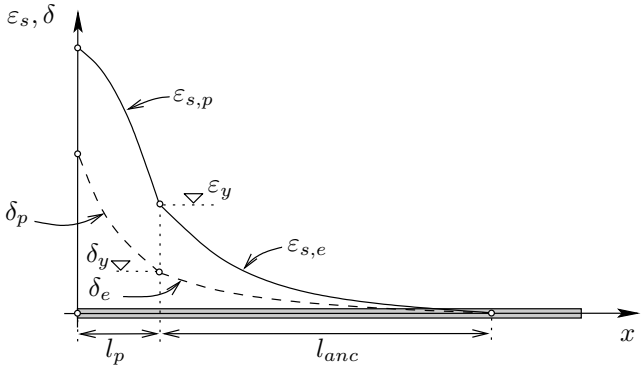

Figure 8

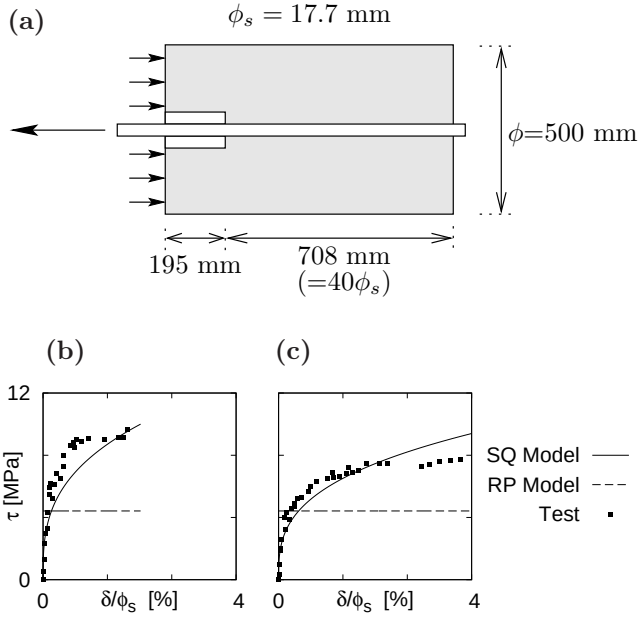

Figure 9

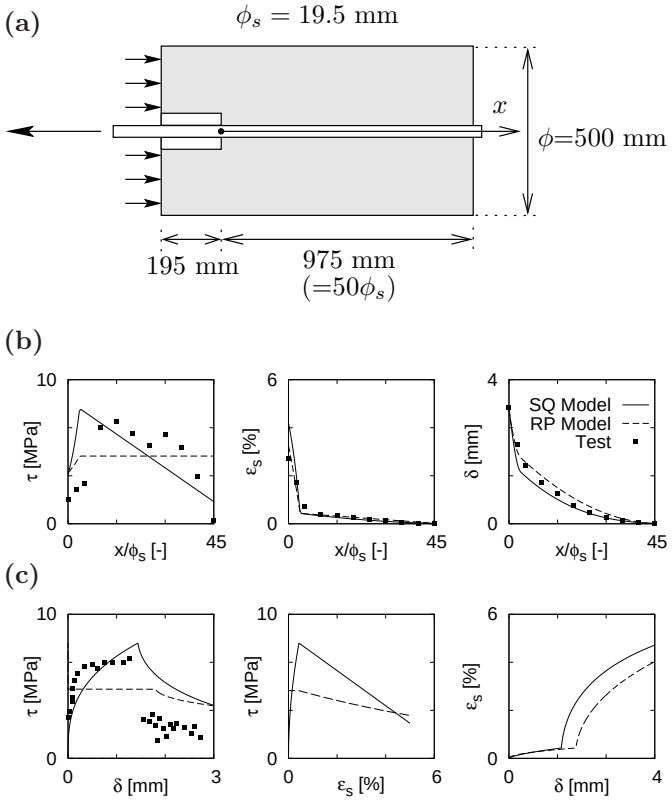

Figure 10

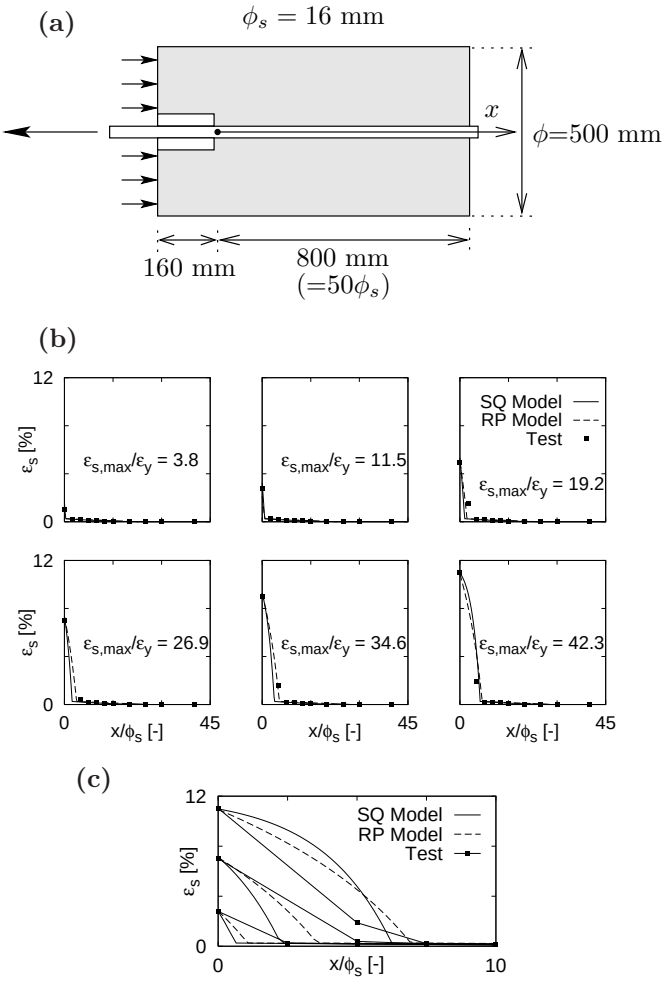
(a)
ϕ_s = 16 mm
x
ϕ=500 mm
160 mm
800 mm
(=50ϕ_s)
(b)
12
ε_s [%]
0
$\varepsilon_{s,max}/\varepsilon_y$ = 3.8
$\varepsilon_{s,max}/\varepsilon_y$ = 11.5
SQ Model
RP Model
Test
$\varepsilon_{s,max}/\varepsilon_y$ = 19.2
$\varepsilon_{s,max}/\varepsilon_y$ = 26.9
$\varepsilon_{s,max}/\varepsilon_y$ = 34.6
$\varepsilon_{s,max}/\varepsilon_y$ = 42.3
0
45
x/ϕ_s [-]
(c)
12
SQ Model
RP Model
Test
ε_s [%]
0
0
x/ϕ_s [-]
10

Figure 11

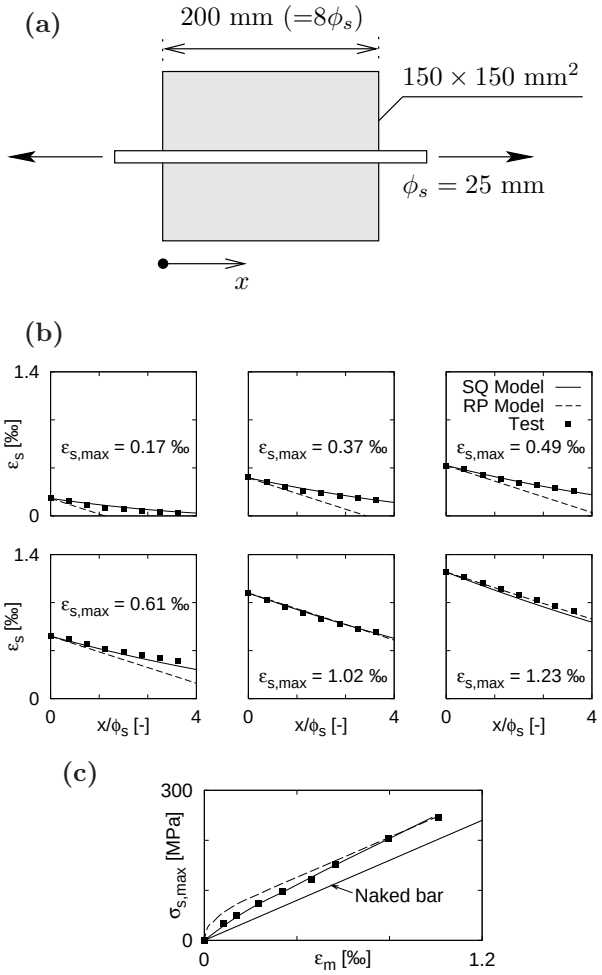
(a)
200 mm (=8ϕ_s)
150 × 150 mm^2
ϕ_s = 25 mm
x
(b)
SQ Model
RP Model
Test
$\varepsilon_{s,max}$ = 0.17 ‰
$\varepsilon_{s,max}$ = 0.37 ‰
$\varepsilon_{s,max}$ = 0.49 ‰
$\varepsilon_{s,max}$ = 0.61 ‰
$\varepsilon_{s,max}$ = 1.02 ‰
$\varepsilon_{s,max}$ = 1.23 ‰
ε_s [‰]
x/ϕ_s [-]
(c)
$\sigma_{s,max}$ [MPa]
Naked bar
ε_m [‰]

Figure 12

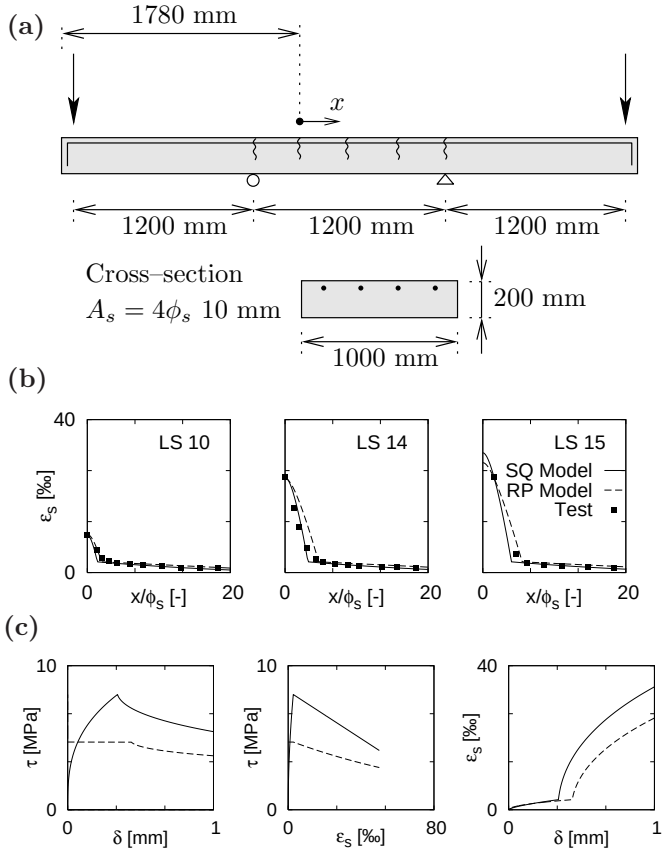

Figure 13

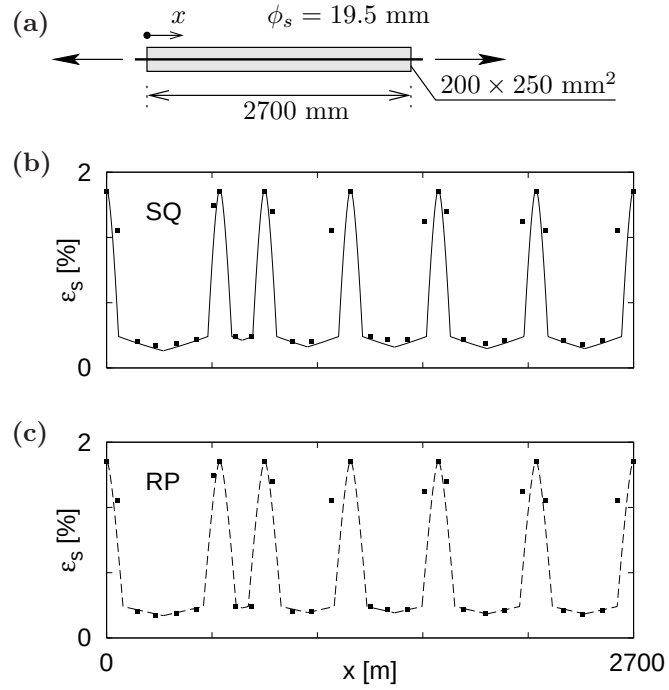

Figure 14